Cation exchange synthesis of CuS nanotubes composed of nanoparticles as low-cost counter electrodes for dye-sensitized solar cells

Xuemin Shuai[a],[*], Wenzhong Shen[b],[*], Xiaoting Li[a], Zhaoyang Hou[a], Sanmin Ke[a], Gang Shi[a], Chunlong Xu[a], Donghua Fan[c]

[a] Department of Applied Physics, Chang'an University, Xi'an 710064, China
[b] Laboratory of Condensed Matter Spectroscopy and Opto-Electronic Physics, and Key Laboratory of Artificial Structures and Quantum Control (Ministry of Education), Department of Physics, Shanghai Jiao Tong University, Shanghai 200240, China
[c] School of Applied Physics and Materials, Wuyi University, 22 Dongcheng Village, Jiangmen 529020, China

ARTICLE INFO

ABSTRACT

In this work, CuS nanotubes composed of nanoparticles with relative high catalytic activity have been successfully synthesized via a facile conversion process from ZnS nanotubes precursors. The successful chemical conversion from ZnS nanotubes to CuS ones could be attributed to a cation exchange process which benefits by the large difference in solubility between ZnS and CuS. A possible formation mechanism and growth process of the CuS nanotubes is discussed based on the experimental results. The as-prepared CuS nanotubes were then used as counter electrodes (CEs) and demonstrated good performance in dye-sensitized solar cells (DSSCs). The good performance is attributed to the increased surface area and the good electrocatalytical activity of CuS. This approach can provide a potent technique to obtain inorganic materials with unique structures and chemical compositions.

1. Introduction

Copper sulfides are a series of compounds with variable stoichiometries of Cu_xS (x = 1–2), and the five stable copper sulfide phases at room temperature are Cu-rich chalcocite (Cu_2S), $Cu_{1.96}S$ (djurleite), $Cu_{1.8}S$ (digenite), $Cu_{1.75}S$ (anilite) and S-rich covellite (CuS) [1]. These copper sulfide materials may find applications in manufacture of high capacity cathode for lithium batteries [2], solar cell devices, solar controllers [3–7], nanometer-scale switches [8] and room temperature ammonia sensors [9]. Among the Cu_xS compounds, copper(II) sulfide (CuS) exhibits its commercial importance as pigment, catalyzer, colored indicator of nigrosine and so on [10]. To date, researchers have attempted in making a variety of nanostructures of CuS such as nanoparticles [11], nanocrystals [12], nanopeas [13], nanorods [14], nanotubes [15], nanocones and nanobelts [16], nanoflakes and nanoplatelets [17] via many synthesis routes, including the template-assisted approach, chemical bath deposited method, microwave method, electrosynthesis, thermolysis and so on [11–20]. Most of these synthetic methods mentioned above involve template, surfactant, or complex equipment and are uncontrollable of chemical composition

and crystal structure. Recently, the developments in chemical conversion and cation exchange offer a promising approach to convert the chemical compositions of nanostructures without destroying the original morphology. Lubeck and Han [21] and Yu and co-workers [22] have successfully synthesized mesostructured CuS and CuS hollow spheres utilizing ion-exchange methods transformed from CdS and ZnS, respectively.

Among various nanostructures, nanotubes and nanoparticles are good candidates for studying the phenomena such as electrical resistivity, strength, magnetic and optical properties due to their enormous surface area, strength and the quantum size. [23–32]. Moreover, based on the requirements of fast electron transport and high active surface area for counter electrodes in dye-sensitized solar cells (DSSCs), the nanotubes and nanoparticles may offer such benefits [33]. Therefore, nanotubes integrated with nanoparticles which possess large amount of nanosized rough surfaces would provide higher electrocatalytic activity owing to the larger surface area, and as we all know that the available catalytic surface in the counter electrode plays a crucial role in determining the overall efficiency of solar cells. Nonetheless, to the best of our knowledge, there are few reports on the

---

controllable synthesis of CuS nanotubes and nanoparticles without using any surfactants or crystal seeds, especially the integration of CuS nanotubes with nanoparticles.

In this regard, we developed a relatively simple, low cost, well-controlled process to prepare large scale of CuS nanotubes composed of nanoparticles at a low temperature of 90 °C. This process involves ZnS nanotubes as a precursor, which is converted to CuS nanotubes via chemical conversion and cation exchange. The key point of the method is to utilize the large difference in solubility between ZnS and CuS for the effective transformation. Moreover, benefiting from the enormous surface area of the nanotubes with rough surface consisted of nanoparticles and good electrocatalytic activity of CuS [34,35], the present CuS nanostructures have been used as the counter electrodes in DSSCs, and exhibited good photovoltaic performances.

Compared with the previous reports, the great success of the work reported in this paper is that a facile, versatile, and economic method has been demonstrated to control and manipulate effectively the chemical compositions and structures of nanotubes integrated with nanoparticles. This method might be applied in industry owing to its simple approach, innocuous reagents, benign to environment, reproducible and high yields. We have further expected that the present strategy might open up an opportunity to synthesize other 1D nanostructure with novel morphologies. In addition, the simple preparation at a low temperature and inexpensive cost of CuS nanotubes with the synergistic catalytic effect of nanoparticles open up new avenues for counter electrodes of DSSCs, and we believe that the current work paves the way for the development of a new generation of highly efficient, low-cost DSSCs using novel counter electrodes.

2. Materials and methods

2.1. Synthesis of nanotubes

2.1.1. Synthesis of ZnS nanotubes

The preparation details for ZnS nanotubes can be found in our recently published papers [36]. In brief, ZnO nanowires were prepared by a hydrothermal process firstly. In a typical preparation, 0.2 g ZnCl$_2$ and 20.0 g Na$_2$CO$_3$ were added into a 50 mL Telfon-lined stainless steel autoclave and filled with distilled water up to 90% of its volume. After vigorous stirring for 30 min, the autoclave was kept at 140 °C for 12 h and then cooled to room temperature naturally. Subsequently, the as-prepared ZnO nanowires were washed and dried, and then were transferred to a Pyrex glass bottle containing 40 mL 0.2 M thioaceta-mide (TAA). The sealed bottle was maintained at 90 °C for 9 h in a conventional laboratory oven to synthesize ZnS nanotubes. The final precipitates were washed repeatedly with deionized water and dried at 60 °C.

2.1.2. Synthesis of CuS nanotubes

To realize the synthesis of CuS nanotubes, the silicon or glass slides with ZnS nanotubes on them were transferred to a Pyrex glass bottle containing 100 mM Cu(NO$_3$)$_2$ and 70 mM tartaric acid (which is to avoid the hydrolyzation of Cu^{2+} in water), and the solution temperature was kept at 90 °C. The final products on the substrates were washed thoroughly using deionized water to remove any co-precipitated salts and then dried at air at 60 °C. For better crystal quality and stability, the obtained CuS nanotubes were annealed at 200 °C for 10 min under argon atmosphere.

2.2. Morphological and structural characterization

The morphology and microstructure were examined using a field-emission scanning electron microscopy (FE-SEM; Philips XL30FEG, FEI Co., Hillsboro, OR, USA) with an accelerating voltage of 5 kV and a high-resolution transmission electron microscopy (HRTEM; JEOL JEM-2100F, JEOL Ltd., Akishima, Tokyo, Japan). Selected area electron

diffraction (SAED) and energy dispersive X-ray (EDX) microanalysis were also performed during the TEM and SEM observations. Powder X-ray diffraction (XRD) analyses were made on a diffractometer (D/max-2200/PC, Rigaku Corporation, Tokyo, Japan) equipped with a high intensity Cu Kα radiation (λ = 1.5418 Å). Raman spectra were measured at room temperature using a Jobin Yvon LabRAM HR 800UV micro-Raman/PL system (HORIBA Jobin Yvon Inc., Edison, NJ, USA) at the backscattering configuration excited with He-Cd laser (325.0 nm) for ZnS nanotubes, but Ar$^+$ laser (514.5 nm) for CuS nanotubes.

2.3. Fabrication of DSSCs

The TiO$_2$ nanoporous films with an area of 0.25 cm^2 were sintered in air for 1 h at 500 °C, and then immersed in 0.5 mM N719 dye (Ruthenium 535-bisTBA) solution in ethanol for 12 h. The CuS-coated FTO glass was prepared by drop-casting CuS solution on the clean FTO glass and subsequently wait until all solvent evaporates. The tested dye sensitized solar cells were front-side illuminated, using TiO$_2$ nanoporous films as photoanodes and CuS nanotubes as counter electrodes. The liquid electrolyte was injected into the cells by a syringe, which consisted of 0.1 M iodine (I$_2$), 0.1 M lithium iodide (LiI), 0.6 M tetra-butylammonium iodide and 0.5 M 4-tert-butyl pyridine in acetonitrile (CH$_3$CN, 99.9%). The platinum-based electrode is prepared by coating FTO glass with a 4 mM H$_2$PtCl$_6$ solution in ethanol and then heating in air at 400 °C for 60 min, while maintaining the same fabrication of TiO$_2$ photoanodes.

3. Results and discussions

3.1. Preparation and characterization of ZnS nanotubes

At first, ZnO nanowires were fabricated by a hydrothermal process in our experiments. Subsequently, to convert ZnO nanowires to ZnS nanotubes, we transferred the ZnO nanowires into a solution containing 0.2 M TAA (which provides sulfide ions), and the solution was kept at 90 °C for 9 h [36]. We believe that this result may be explained by kirkendall effect, which normally refers to comparative diffusive migrations among different atomic species in metals and /or alloys under thermally activated conditions [37]. Fig. 1a is a typical SEM image of ZnS nanotubes. Herein, ZnS nanotubes with open tips can be clearly observed. Fig. 1b is a representative TEM image of the as-prepared product, in which ZnS nanotubes with average diameter of 70 nm can be found. The TEM image gives further evidence for the hollow structure of ZnS nanotubes. Fig. 1c shows a HRTEM image taken on the edge of an individual ZnS nanotube, in which clear crystal lattice fringes without noticeable structural defects can be observed. The corresponding ring-like SAED pattern (inset of Fig. 1c) provides further evidence for the polycrystalline nature of ZnS nanotubes, agreeing well with the HRTEM analysis. EDX spectrum (Fig. 1d) of ZnS nanotubes presents prominent Zn and S peaks (Si peaks are derived from substrates). The XRD pattern (Fig. 1e) indicates that peaks can be indexed to cubic phase of ZnS according to JCPDS card 05-0566. Measurement of the room-temperature Raman spectrum (Fig. 1f) also confirms that the reaction product is ZnS. The observation of multiple resonant Raman peaks indicates that the yielded ZnS nanotubes possess good optical quality [38].

3.2. Preparation and characterization of CuS nanotubes

The ZnS nanotubes were converted to CuS ones by transferring the substrates with ZnS nanotubes on them into 40 mL of 100 mM Cu(NO$_3$)$_2$ and 70 mM tartaric acid aqueous solution. When the pale yellow ZnS nanotubes are immersed into the above-mentioned solutions, the ZnS surface turned blue black immediately, and then shinning cyan and gray in a short time. The color change is an indication that the CuS species is formed. After 1 h's reaction, the product surface became black
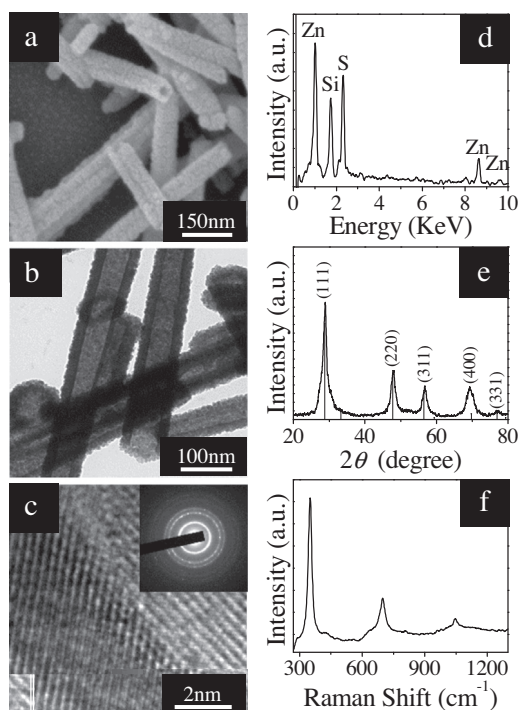
Fig. 1. (a) FE-SEM and (b) TEM images of ZnS nanotubes. (c) HRTEM image of a ZnS nanotube shell, together with the corresponding SAED pattern shown in the inset. The corresponding (d) EDX, (e) XRD, and (f) room-temperature Raman spectra of ZnS nanotubes.
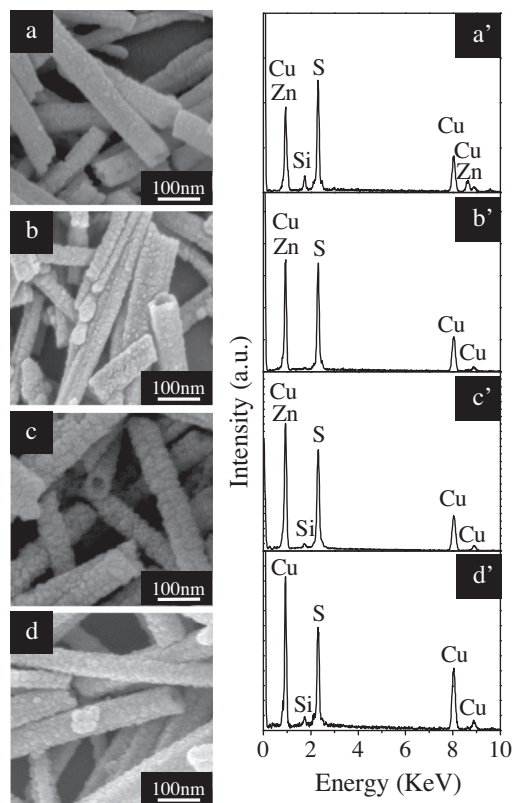

Fig. 2. FE-SEM images of CuS nanotubes with different reaction times: (a) 10 min, (b) 20 min, (c) 40 min, and (d) 1 h; (a'–d') The corresponding EDX of CuS nanotubes with different reaction times.

and fluffy, demonstrating the formation of dense CuS nanotubes. Several time-dependent experiments were carried out to investigate the intermediate transition from ZnS nanotubes to CuS nanotubes and the possible growth mechanism. A series of SEM images in Fig. 2 show the morphology at different reaction stages corresponding to the reaction time of 10, 20, 40 min and 1 h, respectively. When the ZnS nanotubes and $Cu(NO_3)_2$ react at 90 °C for 10 min, some CuS nanoparticles on the ZnS nanotubes are observed because ions exchange happens as Cu^{2+} reacts with S^{2-} slowly dissolved from the surface of ZnS nanotubes to form initial CuS shells, as depicted in Fig. 2a. When prolonging the reaction time to 20 min (shown in Fig. 2b), the nanotube surface becomes more rough, revealing that more CuS nanoparticles piled up on the initial CuS shells. When the reaction time reach to 40 min, large numbers of CuS nanoparticles come into being and arrange along the 1D direction (Fig. 2c). Finally, some well-defined CuS nanotubes composed of nanoparticles with diameters of about 70 nm and lengths of about 300–500 nm appear in Fig. 2d when further prolonging the reaction time to 1 h under hydrothermal conditions.

The corresponding EDX analyses (Fig. 2a'–d') give clear evidence for the FE-SEM observation of the samples obtained at different reaction times. We can observe the successful incorporation of Cu element into the ZnS nanotubes in the compositional information (Fig. 2a'), and the Cu/Zn stoichiometric ratio is 0.51. The signal of Si originates from the substrate. As the reaction progressed, the Cu/Zn stoichiometric ratio becomes higher and higher (from 1.16 to 2.58) on account of that more and more Zn atoms were replaced by Cu atoms, as shown in Fig. 2b'–c'. When the reaction time is extended to 1 h, only Cu, S and Si elements are observed (Fig. 2d'), and the Cu/S stoichiometric ratio is 1.0. This atomic ratio confirms that the nanotubes consist of CuS other than a mixture of copper sulfides with different compositions.

Based on the above experimental observation, the whole process can be described as follows. Once the ZnS nanotubes were transferred into $Cu(NO_3)_2$ solution, cation exchange began at the interfaces between the ZnS nanotube surfaces and solution. As the reaction time went on, Zn^{2+} was gradually substituted by Cu^{2+}, leading to the synthesis of CuS nanotubes. The driving force for the cation exchange is offered by the large difference in solubility between ZnS and CuS (solubility product constant (K_{sp}) of ZnS is 2.93×10^{-25}, whereas K_{sp} of CuS is 5.0×10^{-36}) [39]. The above conversion mechanism manifests that the ZnS nanotubes act both reactants and templates during the cation-exchange process.

In order to follow the morphology evolution of the CuS nanotubes in depth, the products obtained at different reaction stages were collected and characterized by TEM (Fig. 3). The product obtained at 10 min exhibits slightly rough surfaces, indicating the initial deposition of CuS nanocrystallites on the surfaces of the original ZnS nanotubes (Fig. 3a). When the reaction time is increased to 20 min, the layer of deposited CuS nanocrystallites become significantly denser and thicker, suggesting the formation of core-shell-structured ZnS@CuS nanotubes (Fig. 3b). Prolonged reaction times will lead to the formation of numerous CuS nanocrystallites on the outer layers (Fig. 3c). When the reaction is prolonged to 1 h, we are able to realize uniform and pure CuS nanotubes composed of nanoparticles with about 70 nm in diameter and 21 nm in shell-thickness (Fig. 3d).

Fig. 3e displays the HRTEM image for the wall of individual CuS-1 h nanotube. It is obvious that the CuS nanotubes are polycrystalline, and the clearly observed crystal lattice fringes demonstrate that the nanotubes are highly crystallized, and free from dislocation and stacking faults. Moreover, the corresponding SAED pattern with characteristic ring diffractions (the inset of Fig. 3e) also illustrates the polycrystalline feature of the CuS nanotubes.

The crystallinity of as-synthesized CuS-1 h nanotubes was examined by XRD. The XRD pattern shown in Fig. 4a indicates that peaks could be perfectly indexed to a pure single phase of hexagonal CuS according to JCPDS card 06–0464. No peaks of any other phases or impurities were detected from XRD patterns, indicating the high purity of the product.
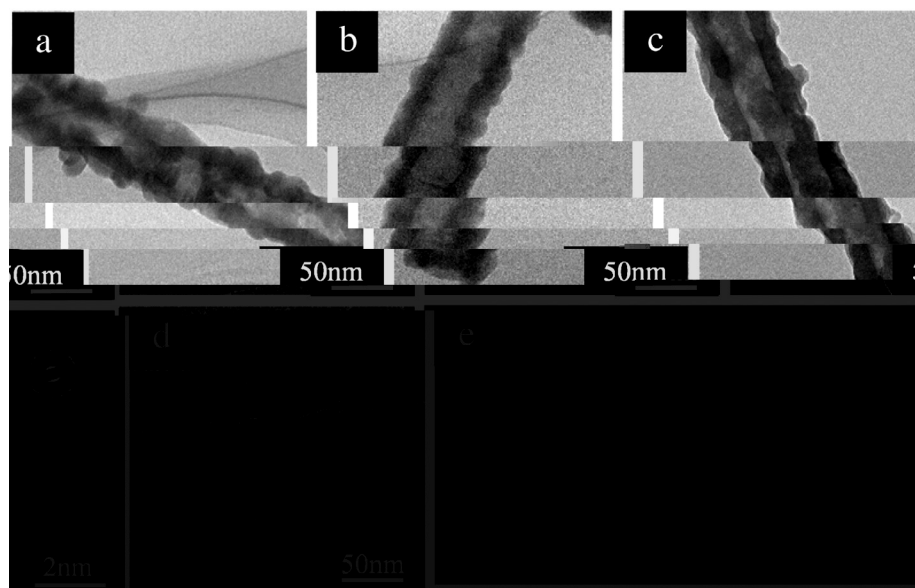
Fig. 3. TEM images of the CuS nanotubes with different reaction times: (a) 10 min, (b) 20 min, (c) 40 min, and (d) 1 h; (e) HRTEM image of the CuS-1 h nanotubes, together with the corresponding SAED pattern shown in the inset.

It has been demonstrated that Raman spectroscopy is a fast and nondestructive tool for appreciating crystalline material qualities. So, structured characterization of the as-synthesized CuS-1 h nanotubes was carried out using Raman spectroscopy. Raman spectrum collected using the 514.5 nm excitation line at room temperature for the CuS-1 h nanotubes is displayed in Fig. 4b. The band centred at $474\,cm^{-1}$ may attributed to the lattice vibration, which is identical to the ones recorded for the corresponding CuS thin films [40,41] and CuS microspheres [42].

3.3. Photovoltaic performances for dye-sensitized solar cells

The effect of the CuS on the cell performance of counter electrodes is illustrated in Fig. 5 and Table 1. Concerning the influence of reaction time on the performance of counter electrodes, a series of time-dependent *J-V* curves are shown in Fig. 5 and the photovoltaic parameters of tested DSSCs are listed in Table 1. As presented in Fig. 5 and Table 1, both short circuit current density (J_{sc}) and open circuit voltage (V_{oc}) increase quickly with increasing the reaction time from 10 min to 1 h, reaching the maximum values of $13.366\,mA\,cm^{-2}$ and 0.64 V at 1 h's reaction time, yielding the highest photovoltaic conversion efficiency (η) of 3.34%. Obviously, with increasing the reaction time, larger specific surface area of produced CuS nanoparticles will help to increase the catalytic reaction sites [43], and the composition of the nanotubes gradually changing from ZnS through mixed ZnCuS to CuS will help to enhance electrocatalytical activity [34,44], thus giving higher J_{sc} and η of the device. As a result, the large surface area and the good electrocatalytical activity of the CuS nanotubes may be the key for the high photovoltaic performance. Furthermore, we have preliminarily evaluated the stability of the DSSC constructed by CuS-1h counter
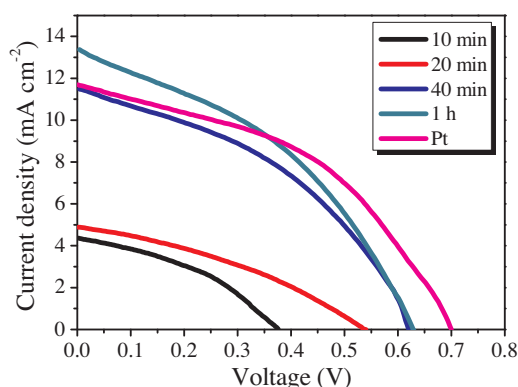

Fig. 5. Photovoltaic behaviour of dye-sensitized solar cells with counter electrodes of Pt and CuS nanotubes at different reaction times, under one sun illumination ($100\,mW\,cm^{-2}$).

Table 1

Photovoltaic parameters of tested DSSCs using Pt and CuS nanotubes of different reaction times as counter electrodes.

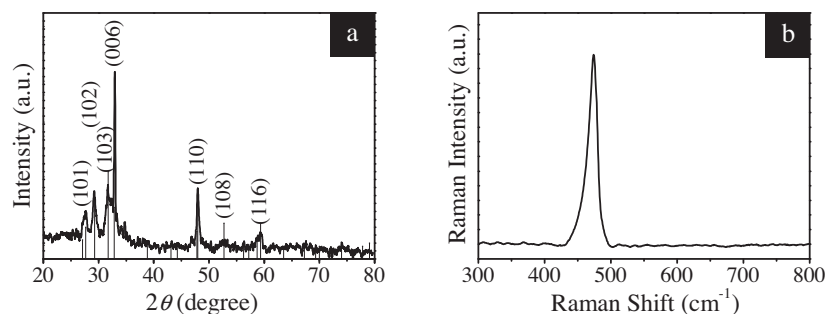|	J_{sc} (mA cm^{-2})	V_{oc} (V)	FF	η (%)
CuS-10 min	4.37	0.38	0.38	0.64
CuS-20 min	4.89	0.54	0.35	0.93
CuS-40 min	11.51	0.62	0.39	2.94
CuS-1 h	13.37	0.64	0.40	3.34
Pt	11.69	0.70	0.44	3.62

Fig. 4. (a) XRD pattern and (b) room-temperature Raman spectrum of the CuS-1 h nanotubes.
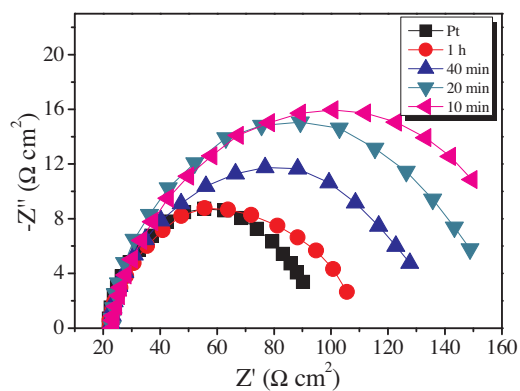
Fig. 6. Nyquist plots of the symmetric cells based on the CuS-10 min, CuS-20 min, CuS-40 min, CuS-1 h, and the Pt counter electrodes.

electrode, which was tested under continuous illumination of $100\,mW\,cm^{-2}$ in working conditions. It is found that the DSSC did not show significant degradation after 10 h, indicating fairly good stability. However, as mentioned before, the current product is black and fluffy, which means the transparency of our CuS nanotubes is relatively poor. Therefore, we are trying our best to improve the transparency of the product in any follow-on work, which is very important in the efficiency of DSSCs.

DSSC fabricated with Pt counter electrode was also tested and the result was shown in Fig. 5 (detailed data showed in Table 1) for comparison. In comparison with CuS nanotubes, although the Pt CE exhibited slightly higher photovoltaic conversion efficiency (η), it's worth noting that decreasing cost is always crucial in the future development of various solar cells, which means our CuS counter electrodes hold great potential for the fabrication of high-efficiency dye-sensitized solar cells. Besides that, we believe by further optimizing the transparency, tube length, annealing temperature and electrolyte composition, the efficiency can be expected to be further improved.

In order to further evaluate the electrochemical characteristics of the as-prepared CuS nanotubes as counter electrodes in DSSCs, electrochemical impedance spectra (EIS) were measured in a symmetric cell configuration consisting of two identical counter electrodes, and the resultant Nyquist plots are illustrated in Fig. 6. From the plots, it could be seen that the CuS-10 min counter electrode demonstrated the largest charge transfer resistance (R_{ct}) ($142.2\,\Omega\,cm^{-2}$), which was attributed to its relatively lower catalytic activity [45]. At the same time, the CuS-20 min ($131.1\,\Omega\,cm^{-2}$), CuS-40 min ($109.9\,\Omega\,cm^{-2}$), and CuS-1 h ($85.5\,\Omega\,cm^{-2}$) counter electrodes presented relatively much lower R_{ct} than that of the CuS-10 min electrode, which accounts for the enhanced photovoltaic performance. Moreover, the value of CuS-1 h is close to that of the Pt ($75.6\,\Omega\,cm^{-2}$) electrode, indicating that CuS-1 h exhibits a decent electrochemical catalytic ability as a counter electrode in the DSSCs. However, the CuS-1 h nanotubes had a slightly higher J_{sc} value than Pt partially since they had larger surface areas to give more catalytic sites for the reaction of I_3^-/I^- ions in electrolytes [46].

4. Conclusions

In summary, a successful morphological transformation of nanotubular ZnS to CuS was achieved at a low temperature of 90 °C. The mechanism by which the cation exchange is owe to the large difference in solubility between ZnS and CuS. The morphologies and structures of the yielded CuS nanotubes composed of nanoparticles were investigated. We have further successfully employed the prepared CuS nanostructures as counter electrodes in dye-sensitized solar cells. The photovoltaic conversion efficiency of 3.34% was obtained with CuS-1h counter electrode due to the increased surface area and the good electrocatalytical activity of CuS. With their low cost and simplicity, we

believe that such DSSCs have great potential for use in next-generation solar cells. Our results show that the present strategy is a versatile route for expanding the range of nanoscale materials with diverse compositions, structures, and shapes without having to develop new synthetic methods to produce each individual nanostructure.

Acknowledgements

Conflicts of interest

None.

References

[1] H.L. Hwang, J.J. Loferski, E.A. DeMeo, R. Beaulieu, Application of luminescence in studies of photovoltaic properties of Cu-Cd-S solar cells, J. Crystal Growth 59 (1982) 425–431.

[2] J.S. Chung, H.J. Sohn, Electrochemical behaviors of CuS as a cathode material for lithium secondary batteries, J. Power Sources 108 (2002) 226–231.

[3] M. Congiu, O. Nunes-Neto, M.L. De Marco, D. Dini, C.F.O. Graeff, Cu₂₋ₓS films as counter-electrodes for dye solar cells with ferrocene-based liquid electrolytes, Thin Solid Films 612 (2016) 22–28.

[4] S. Erokhina, V. Erokhin, C. Nicolini, F. Sbrana, D. Ricci, E.D. Zitti, Microstructure origin of the conductivity differences in aggregated CuS films of different thickness, Langmuir 19 (2003) 766–771.

[5] L. Reijnen, B. Meester, A. Goossens, J. Schoonman, Atomic layer deposition of CuₓS for solar energy conversion, Chem. Vap. Deposition 9 (2003) 15–20.

[6] K.D. Yuan, J.J. Wu, M.L. Liu, L.L. Zhang, F.F. Xu, L.D. Chen, F.Q. Huang, Fabrication and microstructure of p-type transparent conducting CuS thin film and its application in dye-sensitized solar cell, Appl. Phys. Lett. 93 (2008) 132106.

[7] X.J. Zhang, X.Q. Liu, Y.P. Zhang, R.R. Bao, D.F. Peng, T.F. Li, G.Y. Gao, W.X. Guo, C.F. Pan, Rational design of an ITO/CuS nanosheet network composite film as a counter electrode for flexible dye sensitized solar cells, J. Mater. Chem. C 4 (2016) 8130–8134.

[8] T. Sakamoto, H. Sunamura, H. Kawaura, Nanometer-scale switches using copper sulfide, Appl. Phys. Lett. 82 (2003) 3032–3034.

[9] A. Galdikas A. Mironas V. Strazdien A. Šetkus I. Ancutien V. Janickis Room-temperature-functioning ammonia sensor based on solid-state CuxS films. Sens. Actuators B 67 (2000) 76-83.

[10] L. Gao, E.B. Wang, S.Y. Lian, Z.H. Kang, Y. Lan, D. Wu, Microemulsion-directed synthesis of different CuS nanocrystals, Solid State Commun. 130 (2004) 309–312.

[11] K.J. Iwahori, R. Takagi, N.K. Kishimoto, I. Yamashita, A size controlled synthesis of CuS nano-particles in the protein cage, apoferritin, Mater. Lett. 65 (2011) 3245–3247.

[12] X. Liu, X.L. Wang, B. Zhou, W.C. Law, A.N. Cartwright, Mark T. Swihart, Size-controlled synthesis of Cu₂₋ₓE (E = S, Se) nanocrystals with strong tunable near-infrared localized surface plasmon resonance and high conductivity in thin films, Adv. Funct. Mater. 23 (2013) 1256–1264.

[13] H.J. Kim, J.H. Kim, C.H.S.S.P. Kumar, D. Punnoose, S.K. Kim, C.V.V.M. Gopi, S.S. Rao, Facile chemical bath deposition of CuS nano peas like structure as a high efficient counter electrode for quantum-dot sensitized solar cells, J. Electroanal. Chem. 739 (2015) 20–27.

[14] J.F. Guan, J. Peng, X.Y. Jin, Synthesis of copper sulfide nanorods as peroxidase mimics for the colorimetric detection of hydrogen peroxide, Anal. Methods 7 (2015) 5454–5461.

[15] J.R. Huang, Y.Y. Wang, C.P. Gu, M.H. Zhai, Large scale synthesis of uniform CuS nanotubes by a sacrificial templating method and their application as an efficient photocatalyst, Mater. Lett. 99 (2013) 31–34.

[16] C.L. Jiang, W.Q. Zhang, G.F. Zou, L.Q. Xu, W.C. Yu, Y.T. Qian, Hydrothermal fabrication of copper sulfide nanocones and nanobelts, Mater. Lett. 59 (2005) 1008–1011.

[17] A.D. Savariraj, K.K. Viswanathan, K. Prabakar, CuS nano flakes and nano platelets as counter electrode for quantum dots sensitized solar cells, Electrochim. Acta 149 (2014) 364–369.

[18] H. Li, Y.H. Wang, J.X. Huang, Y.Y. Zhang, J.B. Zhao, Microwave-assisted synthesis of CuS/Graphene composite for enhanced lithium storage properties, Electrochim. Acta 225 (2017) 443–451.

[19] M. Shamsipur, S.M. Pourmortazavi, M. Roushani, S.S. Hajimirsadeghi, Electrochemical preparation and thermal characterization of copper sulfide nanoparticles, Synth. React. Inorg. Metal-organic 44 (2014) 951–958.

[20] T.H. Larsen, M. Sigman, A. Ghezeibash, R.C. Doty, B.A. Korgel, Solventless synthesis of copper sulfide nanorods by thermolysis of a single source thiolate-derived precursor, J. Am. Chem. Soc. 125 (2003) 5638–5639.

[21] C.R. Lubeck, T.Y.J. Han, A.E. Gash, J.H. Satcher Jr, F.M. Doyle, Synthesis of mesostructured copper sulfide by cation exchange and liquid-crystal templating, Adv. Mater. 18 (2006) 781–784.

[22] J.G. Yu, J. Zhang, S.W. Liu, Ion-exchange synthesis and enhanced visible-light photoactivity of CuS/ZnS nanocomposite hollow spheres, J. Phys. Chem. C 114 (2010) 13642–13649.

[23] Q. Liu, J.Q. Tian, W. Cui, P. Jiang, N.Y. Cheng, A.M. Asiri, X.P. Sun, Carbon nanotubes decorated with CoP nanocrystals: a highly active non-noble-metal nanohybrid electrocatalyst for hydrogen evolution, Angew. Chem. 126 (2014) 6828–6832.

[24] J.T. Hu, T.W. Odom, C.M. Lieber, Chemistry and physics in one dimension: synthesis and properties of nanowires and nanotubes, Acc. Chem. Res. 32 (1999) 435–445.

[25] Y. Divon, R. Levi, J. Garel, D. Golberg, R. Tenne, A. Y'aakobovitz, E. Joselevich, Torsional resonators based on inorganic nanotubes, Nano Lett. 17 (2017) 28–35.

[26] R. Levi, O. Bitton, G. Leitus, R. Tenne, E. Joselevich, Field-effect transistors based on WS_2 nanotubes with high current-carrying capacity, Nano Lett. 13 (2013) 3736–3741.

[27] S.A. Wadhwani, U.U. Shedbalkar, R. Singh, M.S. Karve, B.A. Chopade, Novel polyhedral gold nanoparticles: green synthesis, optimization and characterization by environmental isolate of *Acinetobacter* sp. SW30, World J. Microbiol. Biotechnol. 30 (2014) 2723–2731.

[28] E.J. Popczun, C.G. Read, C.W. Roske, N.S. Lewis, R.E. Schaak, Highly active electrocatalysis of the hydrogen evolution reaction by cobalt phosphide nanoparticles, Angew. Chem. 126 (2014) 1–5.

[29] G. Calogero, P. Calandra, A. Irrera, A. Sinopoli, I. Citro, G.D. Marco, A new type of transparent and low cost counter-electrode based on platinum nanoparticles for dye-sensitized solar cells, Energy Environ. Sci. 4 (2011) 1838–1844.

[30] K. Cho, S.H. Han, M.P. Suh, Copper-organic framework fabricated with CuS nanoparticles: synthesis, electrical conductivity, and electrocatalytic activities for oxygen reduction reaction, Angew. Chem. 128 (2016) 1–7.

[31] D.S. Kong, H.T. Wang, Z.Y. Lu, Y. Cui, $CoSe_2$ nanoparticles grown on carbon fiber paper: an efficient and stable electrocatalyst for hydrogen evolution reaction, J. Am. Chem. Soc. 136 (2014) 4897–4900.

[32] A. Eftekhari, V.J. Babu, S. Ramakrishna, Photoelectrode nanomaterials for photoelectrochemical water splitting, Int. J. Hydrogen Energy 42 (2017) 11078–11109.

[33] H.W. Zhu, H.F. Zeng, V. Subramanian, C. Masarapu, K.H. Hung, B.Q. Wei, Anthocyanin-sensitized solar cells using carbon nanotube films as counter electrodes, Nanotechnology 19 (2008) 465204.

[34] Z.S. Yang, C.Y. Chen, C.W. Liu, C.L. Li, H.T. Chang, Quantum dot-sensitized solar cells featuring CuS/CoS electrodes provide 4.1% efficiency, Adv. Energy Mater. 1 (2011) 259–264.

[35] S.S. Kalanur, S.Y. Chae, O.S. Joo, Transparent $Cu_{1.8}S$ and CuS thin films on FTO as efficient counter electrode for quantum dot solar cells, Electrochim. Acta 103 (2013) 91–95.

[36] X.M. Shuai, W.Z. Shen, A facile chemical conversion synthesis of ZnO/ZnS core/shell nanorods and diverse metal sulfide nanotubes, J. Phys. Chem. C 115 (2011) 6415–6422.

[37] A.D. Smigelskas, E.O. Kirkendall, Zinc diffusion in alpha brass, Trans. AIME 171 (1947) 130–142.

[38] Y.F. Zhu, D.H. Fan, W.Z. Shen, Chemical conversion synthesis and optical properties of metal sulfide hollow microspheres, Langmuir 24 (2008) 11131–11136.

[39] R.C. Weast, CRC Handbook of Chemistry and Physics, 69th ed., CRC Press, Boca Raton, 1988.

[40] B. Minceva-Sukarova, M. Najdoski, I. Grozdanov, C.J. Chunnilall, Raman spectra of thin solid films of some metal sulfides, J. Mol. Struct. 410–411 (1997) 267–270.

[41] S.Y. Wang, W. Wang, Z.H. Lu, Asynchronous-pulse ultrasonic spray pyrolysis deposition of $Cu_xS(x = 1, 2)$ thin films, Mater. Sci. Eng., B 103 (2003) 184–188.

[42] S. Xu, Q. Wang, J.H. Cheng, Q.H. Meng, Y. Jiao, Preparation and characteristics of porous CuS microspheres consisted of polycrystalline nanoslices, Powder Technol. 199 (2010) 139–143.

[43] M.H. Deng, Q.X. Zhang, S.Q. Huang, D.M. Li, Y.H. Luo, Q. Shen, T. Toyoda, Q.B. Meng, Low-cost flexible nano-sulfide/carbon composite counter electrode for quantum-dot-sensitized solar cell, Nanoscale Res. Lett. 5 (2010) 986–990.

[44] Z.S. Yang, C.Y. Chen, C.W. Liu, H.T. Chang, Electrocatalytic sulfur electrodes for CdS/CdSe quantum dot-sensitized solar cells, Chem. Commun. 46 (2010) 5485–5487.

[45] D. Li, L. Cheng, Y. Zhang, Q. Zhang, X. Huang, Y. Luo, Q. Meng, Development of Cu_2S/carbon composite electrode for CdS/CdSe quantum dot sensitized solar cell modules, Sol. Energy Mater. Sol. Cells 120 (2014) 454–461.

[46] M.D. Ye, X.R. Wen, N. Zhang, W.X. Guo, X.Y. Liu, C.J. Lin, In situ growth of CuS and $Cu_{1.8}S$ nanosheet arrays as efficient counter electrodes for quantum dotsensitized solar cells, J. Mater. Chem. A 3 (2015) 9595–9600.